ACS Catalysis

Subscriber access provided by University of South Dakota

Article

Highly Active and Selective RuPd Bimetallic NPs for the Cleavage of Diphenyl Ether C-O bond

Miao Guo, Juan Peng, Qihua Yang, and Can Li

ACS Catal., **Just Accepted Manuscript** • Publication Date (Web): 22 Oct 2018

Downloaded from http://pubs.acs.org on October 22, 2018

Just Accepted

"Just Accepted" manuscripts have been peer-reviewed and accepted for publication. They are posted online prior to technical editing, formatting for publication and author proofing. The American Chemical Society provides "Just Accepted" as a service to the research community to expedite the dissemination of scientific material as soon as possible after acceptance. "Just Accepted" manuscripts appear in full in PDF format accompanied by an HTML abstract. "Just Accepted" manuscripts have been fully peer reviewed, but should not be considered the official version of record. They are citable by the Digital Object Identifier (DOI®). "Just Accepted" is an optional service offered to authors. Therefore, the "Just Accepted" Web site may not include all articles that will be published in the journal. After a manuscript is technically edited and formatted, it will be removed from the "Just Accepted" Web site and published as an ASAP article. Note that technical editing may introduce minor changes to the manuscript text and/or graphics which could affect content, and all legal disclaimers and ethical guidelines that apply to the journal pertain. ACS cannot be held responsible for errors or consequences arising from the use of information contained in these "Just Accepted" manuscripts.

ACS Publications

is published by the American Chemical Society. 1155 Sixteenth Street N.W., Washington, DC 20036

Published by American Chemical Society. Copyright © American Chemical Society. However, no copyright claim is made to original U.S. Government works, or works produced by employees of any Commonwealth realm Crown government in the course of their duties.

Highly Active and Selective RuPd Bimetallic NPs for the Cleavage of Diphenyl Ether C-O bond

Miao Guo,[a,b] Juan Peng,[a,b] Qihua Yang,[a] Can Li[a]**

[a]State Key Laboratory of Catalysis, iChEM, Dalian Institute of Chemical Physics, Chinese Academy of Sciences, Dalian 116023, People's Republic of China

[b]University of Chinese Academy of Sciences, Beijing 100039, People's Republic of China

ABSTRACT: The cleavage of C-O linkages of aryl ethers into aromatic platform compounds is a challenge reaction but of great importance for sustainable future. Herein, we reported the efficient H_2 assisted C-O bond cleavage of diphenyl ether (DPE) in aqueous phase over ultrasmall RuPd bimetallic NPs supported on amine-rich silica hollow nanospheres (NH_2-SiO_2). $RuPd_5/NH_2$-SiO_2 with TOF of 172 h^{-1} and C-O cleavage selectivity of 99% outperformed the corresponding monometallic counterparts and is among the most active solid catalysts for C-O bond cleavage of DPE. The control experiments and characterization results showed that the effective isolation of Ru sites and optimized H_2 dissociation ability mainly contributed to the enhanced catalytic performance of RuPd bimetallic NPs, in which Ru and Pd worked cooperatively with Ru sites for DPE activation and Pd sites for H_2 dissociation. The alloying two

or multi metal atoms provides an efficient approach for designing high performance catalysts for chemical transformations.

KEYWORDS: biomass, RuPd, bimetallic alloy, diphenyl ether, hydrogenolysis, hydrolysis.

1. INTRODUCTION

Lignin composing nearly 30% of non-fossil organic carbon on Earth is an important aromatic biopolymer.[1] Transformation of lignin and its derivatives into fuels and chemicals is of great importance for sustainable future.[2] Up to date, cleavage of C-O linkages, accounting for two-thirds to three-quarters of all linkages in lignin, using H_2 over metal catalysts is regarded as an effective way to transform lignin into aromatic platform compounds.[3]

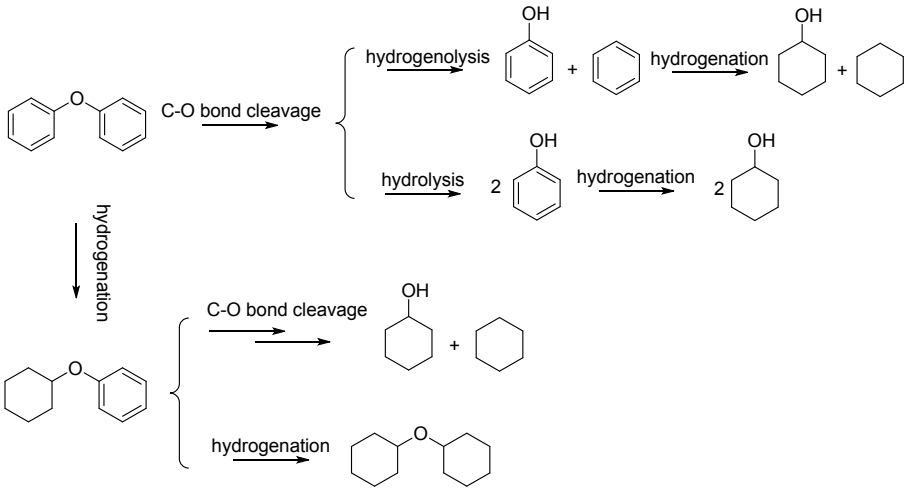

Scheme 1. Summarized possible reaction pathways of H_2 assisted C-O bond cleavage of diphenyl ether in water on the basis of literature reports.

The 4-O-5 linkage (bond dissociation energy of 314 kJ mol^{-1}) is among the strongest and abundant C-O bonds in lignin.[1b,4] Diphenyl ether (DPE) was generally selected as the simplest model compound of 4-O-5 linkage to investigate the C-O bond cleavage chemistry. Hydrogen

assisted DPE cleavage over homogeneous or heterogeneous metal catalysts is very complicated.[5] Generally, it involves competitive hydrogenolysis, (reductive) hydrolysis and hydrogenation on a heterogeneous metal surface in water (**Scheme 1**).[5b,5c]

Due to the complicated reaction pathways, selective cleavage of C-O bond of DPE is very challenge. One of the breakthroughs was made by Sergeev et al. and they obtained 99% selectivity to C-O bond cleavage using N-heterocyclic carbene complex for hydrogenolysis of DPE in the presence of NaO^tBu.[6] In view of the product separation, catalysts handling and reusability, a heterogeneous catalytic process is more attractive. Solid catalysts based on Pd,[5b,7] Pt,[8] Rh,[9] Ru,[10] Ni,[5c,11] and bimetallic catalysts[12] were developed for cleavage the C-O bond of DPE in traditional solvents or in the supercritical CO_2-H_2O medium. TiN-Ni was reported to be efficient for selective hydrogenolysis of diaryl ethers, however, only 58% selectivity to C-O bond cleavage product was obtained using a batch reactor at 125 ^oC for DPE.[11d] Lercher et al.[5b] reported reductive hydrolysis of DPE with C-O bond cleavage selectivity of 90% (88% reductive hydrolysis selectivity and 2% hydrogenolysis selectivity) using Pd/C as a catalyst at 200 °C and 40 bar H_2. Though different types of solid catalysts have been reported, their selectivity and activity towards C-O bond cleavage of DPE still need to be further improved, especially under mild reaction conditions.

To improve the selectivity of C-O bond cleavage, the hydrogenation of aromatic ring of aryl ether should be inhibited due to the fully or partially hydrogenated dimeric compounds ((cyclohexyloxy)benzene (CHPE) and dicyclohexyl ether (DCHE) in DPE transformation) do not easily go further C-O bond cleavage.[5c,11a] The straightforward approach to improve C-O bond cleavage selectivity of DPE is to tune the electronic and surface structure of metal nanoparticles (NPs) by alloying.[13] Bimetallic nanocatalysts usually exhibit improved catalytic

performance over their monometallic counterparts because the combination of two metal atoms could not only induce electronic and geometric effect but also generate the synergistic effect.[14] Previously, the promotion effect of Ni-based bimetallic nanocatalysts[10d,12b,12d] have been reported for C-O bond cleavage of aryl ether, however, the activity and selectivity is still not very high possibly due to the intrinsic property of Ni.

Herein, RuPd bimetallic nanocatalysts were chosen for C-O bond cleavage of DPE considering that Ru NPs are very active in hydrogenolysis reactions and Pd NPs possess high H_2 activation ability.[15] The RuPd/NH_2-SiO_2 exhibited remarkably enhanced activity and selectivity in comparison with Ru/NH_2-SiO_2 and Pd/NH_2-SiO_2. The alloying effect on the catalytic performance of RuPd/NH_2-SiO_2 was elucidated using RuAu/NH_2-SiO_2 as the control catalysts and characterizations such as the XPS, in situ FT-IR of CO adsorption and H_2-D_2 exchange experiments.

2. RESULTS AND DISCUSSION

Our group reported previously that amine groups have high binding affinity for metal cations to afford ultrafine metal NPs.[16] Here, amine-rich silica hollow nanospheres (NH_2-SiO_2) were used as supports, which were prepared via one-pot synthesis method with tetraethoxysilane (TEOS) and (3-aminopropyl)triethoxysilane (APTES) as silane precursors. The characterization results showed that NH_2-SiO_2 hollow nanospheres with particle size of 100~200 nm had the Brunauer-Emmett-Teller (BET) surface area of 156 m^2 g^{-1}, pore size of 15 nm and N content of 3.85 mmol g^{-1} (**Figure S1-S3** and **Table S1**).

$RuPd_x$ bimetallic NPs were deposited on NH_2-SiO_2 by the wet impregnation method using $NaBH_4$ as reductant (x denotes Pd/Ru molar ratio). ICP-AES analysis showed the metal contents of $RuPd_x$/NH_2-SiO_2 were almost the same as expected (**Table S2**). The TEM images clarified the

uniform distribution of $RuPd_x$ NPs on NH_2-SiO_2 (**Figure 1, Figure S4** and **Figure S5**). The particle size of Ru was ~2.5 nm and $RuPd_x$ had relatively smaller particle size of ~2.0 to ~2.2 nm, which is possibility due to the strong interaction between the amine groups and metal cations.[17] In the following discussion, the influence of particle size could be excluded. The High-angle annular dark field scanning transmission electron microscopy (HAADF-STEM) image of the representative $RuPd_5/NH_2$-SiO_2 further confirmed that $RuPd_5$ NPs (~2.1 nm) are uniformly dispersed on NH_2-SiO_2 (**Figure 1D**). The energy dispersive X-ray spectroscopy (EDS) results also showed that the Ru and Pd are homogeneously distributed on NH_2-SiO_2 (**Figure 1F and 1G**). The lattice fringes of $RuPd_5/NH_2$-SiO_2 is 0.220 nm, which is in agreement with the (111) crystal plane of Pd. It seems that the face centered cubic packing structure of Pd is unaffected by alloying with Ru, possibly because of large difference in reduction kinetics and big miscibility gap between Pd and Ru.[18] EDS line scanning analysis verified that the Ru atoms were enriched on the surface of $RuPd_5$ NPs (**Figure S7**).

All catalysts are active toward C-O bond cleavage of DPE with monomers (benzene, cyclohexane, cyclohexanol, cyclohexone and phenol) as main products and dimers, cyclohexyl ether (CHPE) and dicyclohexyl ether (DCHE), as by products (**Figure 2A** and **Table S3**). CHPE and DCHE were generated by hydrogenation of aromatic ring of DPE without C-O bond cleavage. Compounds containing one C6 ring structure derived from C-O bond cleavage were denoted as monomers. In the following discussion, the selectivity to C-O bond cleavage designated monomers selectivity. Ru/NH_2-SiO_2 afforded 36% conversion with 94% selectivity to monomers and Pd/NH_2-SiO_2 gave only negligible conversion (6%) and low selectivity (36%). $RuPd_x/NH_2$-SiO_2 (x = 1, 5, 9) exhibited obviously enhanced activity over Ru/NH_2-SiO_2 or Pd/NH_2-SiO_2, showing the positive effect of alloying Ru and Pd with appropriate Pd/Ru ratio.

The apparent activation energies of H_2 assisted DPE cleavage were measured to be 49 kJ mol^{-1} and 43 kJ mol^{-1} respectively for Ru/NH_2-SiO_2 and $RuPd_5/NH_2$-SiO_2 on the basis of the Arrhenius plots (**Figure S9**), further confirming the above results. The selectivity to monomers of Ru/NH_2-SiO_2 and $RuPd_x/NH_2$-SiO_2 (x = 0.33, 1) is similar and varied in the range of 94-96%. $RuPd_x/NH_2$-SiO_2 (x = 5, 9) afforded the highest monomers selectivity of 99%. $RuPd_{20}/NH_2$-SiO_2 only afforded selectivity of 87%. This suggests that the high monomers selectivity could be obtained within a narrow range of Pd/Ru ratio.

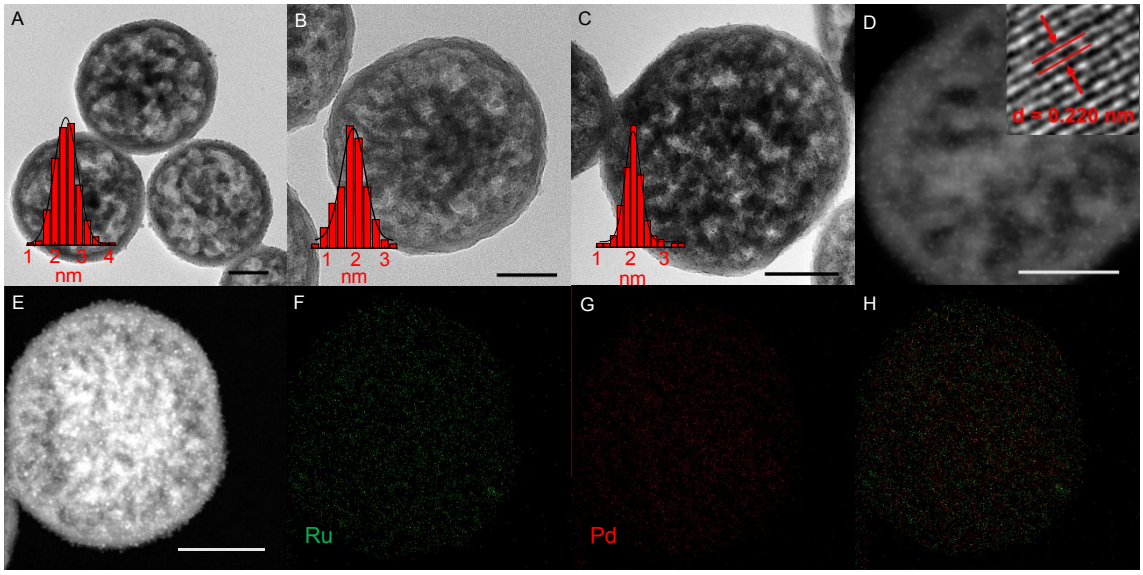

Figure 1. TEM images of (A) Ru/NH_2-SiO_2, (B) Pd/NH_2-SiO_2 and (C) $RuPd_5/NH_2$-SiO_2. (D) and (E) The HAADF-STEM image of $RuPd_5/NH_2$-SiO_2. (F) Ru and (G) Pd STEM-EDS maps for the panel E of $RuPd_5/NH_2$-SiO_2. (H) Reconstructed overlay images of the maps shown in panels F and G: green, Ru; red, Pd. The insets in (A), (B) and (C) show particle size distribution and the inset in (D) for lattice fringe (scale bar 50 nm).

Due to the low activity of Pd/NH_2-SiO_2, the apparent TOF values (TOF_{Ru}) were calculated on the basis of the Ru contents. As shown in **Figure 2B**, the TOF increased sharply as Ru contents decreased. $RuPd_5/NH_2$-SiO_2 with TOF of 172 h^{-1} and up to 99% selectivity to C-O bond cleavage

is the most active and selective solid catalyst ever reported for catalytic cleavage of DPE (**Table S4**). The catalytic cleavage of DPE was also performed at 80 °C (**Figure 2B** and **Table S5**). At this temperature, Pd/NH_2-SiO_2 showed almost no activity, while $RuPd_x/NH_2$-SiO_2 could efficiently catalyze the reaction with $RuPd_5/NH_2$-SiO_2, suggesting that Ru was the active site for DPE cleavage. The activity and selectivity of $RuPd_x/NH_2$-SiO_2 at 80 °C followed the same sequence as those at 110 °C, further confirming the enhancement effect of RuPd alloy.

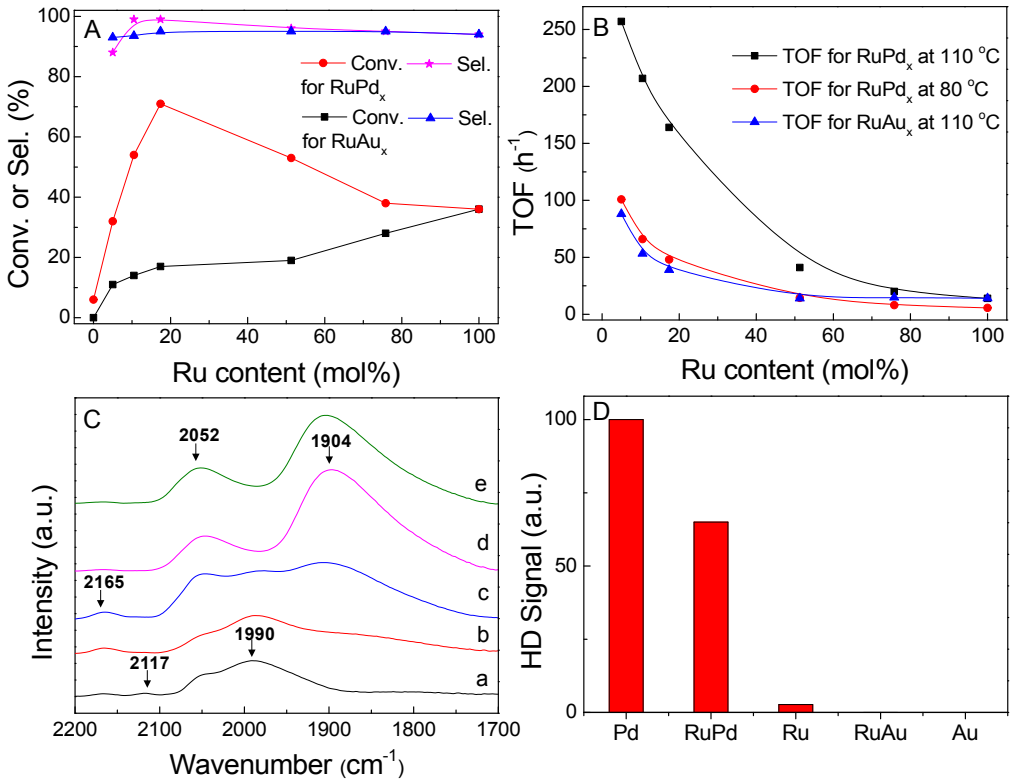

Figure 2. (A) Variation of the DPE conversion and monomers selectivity obtained from RuM_x/NH_2-SiO_2 (M = Pd or Au) catalysts as a function of Ru contents (mol%). (B) The relation of TOF with M/Ru (M = Pd or Au) ratio in aqueous H_2 assisted C-O bond cleavage of DPE over RuM_x/NH_2-SiO_2. (C) In situ FT-IR spectra of CO adsorption on (a) Ru/NH_2-SiO_2, (b) $RuPd_{0.33}/NH_2$-SiO_2, (c) $RuPd_1/NH_2$-SiO_2, (d) $RuPd_5/NH_2$-SiO_2 and (e) Pd/NH_2-SiO_2. (D) H_2-D_2

exchange reactions results on Pd/NH_2-SiO_2, $RuPd_5/NH_2$-SiO_2, Ru/NH_2-SiO_2, $RuAu_5/NH_2$-SiO_2 and Au/NH_2-SiO_2.

Generally, the alloy effects may alter the geometric and electronic properties of the metal NPs.[19] Firstly, the binding energy of Pd 3d and Ru 3p are measured using the X-ray photoelectron spectroscopy (XPS) technique (**Figure S9, Table S7**). In comparison with Ru/NH_2-SiO_2, the Ru 3p binding energies of $RuPd_x/NH_2$-SiO_2 shifted to lower energy. The blue shift of Pd 3d binding energies of $RuPd_x/NH_2$-SiO_2 (x = 0.33, 1) was observed in comparison with Pd/NH_2-SiO_2. The Ru^0 content increased gradually along with the Pd content and reached a plateau at $RuPd_5$ and the Pd^0 concentration for $RuPd_{0.33}$ and $RuPd_1$ is much lower, indicating Pd greatly promoted the reduction of Ru^{n+}.[20] The XPS data indicated the electron transfer from Pd to Ru and the electronic state of $RuPd_x$ NPs differs from those of monometallic NPs because of the strong interaction of Ru and Pd.[20a,21]

The surface structure and composition of $RuPd_x/NH_2$-SiO_2 which may affect their catalytic performance[22] were investigated using in situ FT-IR of CO adsorption considering that the C-O stretching frequency is sensitive to the change on the metal surface where CO is bonded (**Figure 2C, Figure S11**). For Pd/NH_2-SiO_2, the bridge-bonded CO on Pd surface could be observed at 1904 cm^{-1} and the linear-bonded CO occurred at 2052 cm^{-1}. The CO adsorption on Ru/NH_2-SiO_2 is quite complicated with the bands at 2165, 2117 and 2052 cm^{-1} assigned to CO bonded on Ru^{n+}, the band at 1990 cm^{-1} derived from linear CO on Ru^0 surrounded by Ru^{n+} and the weak and broad band at 1815 cm^{-1} for the bridge bonded CO on Ru^0.[23] With Pd content increasing, the bands assigned to CO adsorbed on Ru NPs become less discernible accompanied by the enhancement in the intensity of the CO bands adsorbed on Pd NPs. The bands assigned to CO adsorbed on Ru surface disappeared completely for $RuPd_x/NH_2$-SiO_2 ($x \geq 5$). This is possibly

due to the dilution and isolation of Ru by Pd with $x \geq 5$. On the basis of the *d*-band center theory,[24] the change in the electronic[25] and geometric[26] structure of $RuPd_x$ may modulate the stength of the metal-adsorbate interaction and consquently tailoring their catalytic functions.

The almost linear increase in apparent TOF of $RuPd_x/NH_2$-SiO_2 with x increasing indicates that the isolated Ru sites are more active for DPE cleavage. The dilution of Ru by Pd is an ensemble effect of alloying, which is often observed in the AuPd bimetallic system.[13b] On the basis of the XPS results, the Pd also modifies the electronic properties of Ru. To verify the role of Pd in $RuPd_x/NH_2$-SiO_2, control samples, $RuAu_x/NH_2$-SiO_2 (metal loading content of 4 wt% and x denotes the Au/Ru molar ratio, the particle size of ~2.2 nm, **Figure S6**), were prepared. The EDS results show that the existence of Ru and Au on NH_2-SiO_2 (**Figure S7**). Based on the EDS line scanning, the RuAu alloy may have a Ru surface enriched structure (**Figure S8B**).[27]

XPS data showed that the binding energies of Ru 3p and Au 4f of $RuAu_x/NH_2$-SiO_2 are almost similar to corresponding Ru/NH_2-SiO_2 and Au/NH_2-SiO_2, showing the weak interactions between Ru and Au (**Table S8**).[28] The in situ FT-IR spectra of CO adsorbed on $RuAu_x/NH_2$-SiO_2 resemble that of Ru/NH_2-SiO_2 due to the weak adsorption of CO on Au NPs (**Figure S11**). The red shift in bands assigned to CO adsorbed on Ru^0 surrounded by Ru^{n+} was observed for $RuAu_x/NH_2$-SiO_2 (x = 5, 9 and 20), possibly due to the weak interaction of dipole-dipole coupling between CO molecules on metal surface.[29] The intensity of CO adsorption band decreases as Ru content decreasing and the band disappears almost completely for $RuAu_5/NH_2$-SiO_2, suggesting that the effective isolation of Ru by Au was achieved with $x \geq 5$. The above results show that the alloying Ru with Au only induced the site isolation of Ru.[30]

No activity was observed for Au/NH_2-SiO_2 in the cleavage of DPE and $RuAu_x/NH_2$-SiO_2 could efficiently catalyze this reaction with monomers selectivity varying in the range of 95% to

93% (**Figure 2A**). The activity of $RuAu_x/NH_2$-SiO_2 was much lower than that of $RuPd_x/NH_2$-SiO_2. In the contrary to $RuPd_x/NH_2$-SiO_2, the conversion decreases gradually as the Ru contents decreases though the TOF of $RuAu_x/NH_2$-SiO_2 (x = 5, 9 and 20) increased with the Ru contents decreasing. This suggests that the site isolation of Ru is not the main reason for the enhanced catalytic performance of $RuPd_x/NH_2$-SiO_2.

The activation of H_2 on metal surfaces was tested using H_2-D_2 exchange measurement considering that the H_2 activation/dissociation is one of the important element steps in hydrogenation/hydrogenolysis reactions[31] (**Figure 2D**). The normalized activity followed the order of Pd/NH_2-SiO_2 (100) > $RuPd_5/NH_2$-SiO_2 (65) > Ru/NH_2-SiO_2 (2.7) > $RuAu_5/NH_2$-SiO_2 (0.03) > Au/NH_2-SiO_2 (~0). The activity of $RuPd_5/NH_2$-SiO_2 is 24 times that of Ru/NH_2-SiO_2. The significantly enhanced H_2 activation ability of $RuPd_5/NH_2$-SiO_2 may be due to the electronic effect of RuPd alloy and superior hydrogen dissociation capabilities of Pd.[15c, 32] On the contrary, $RuAu_5/NH_2$-SiO_2 exhibit inferior catalytic performance due to the low activation ability of the Au NPs.[33] On the basis of kinetic studies, a 0.64-order dependence of H_2 and the large KIE effect (K_H/K_D = 3.1) was observed for $RuPd_5/NH_2$-SiO_2 (**Figure S12**), suggesting the dissociation adsorption of H_2 may be involved in the rate-limiting step in the hydrogenation and hydrogenolysis reactions.[11a,34] In correlation of the H_2 activation ability and catalytic performance, it could be seen that $RuPd_5/NH_2$-SiO_2 with moderate H_2 activation ability showed the highest activity and selectivity. Thus, the high catalytic performance of $RuPd_5/NH_2$-SiO_2 could be possibility attributed to the combined effect of optimized H_2 activation ability and site isolation of Ru.

With $RuPd_5/NH_2$-SiO_2 as a model catalyst, the product selectivity as a function of reaction time was investigated (**Table 1**). The DPE conversion increased steadily with reaction time and

approached 99% in 60 min. Benzene, cyclohexanol and cyclohexanone together with a small amount of phenol were detected in initial 3 min. No phenol was detected after 15 min because of its high hydrogenation activity on $RuPd_5/NH_2$-SiO_2. The selectivity to cyclohexane and cyclohexanol increased while the selectivity to benzene and cyclohexanone decreased as the reaction time was prolonged. This indicated that benzene, phenol and cyclohexanone were hydrogenated into saturated products, cyclohexane and cyclohexanol. Only 1% CHPE was detected throughout the whole reaction process, suggesting that CHPE is not the intermediate for C-O bond cleavage of DPE. This was further confirmed by poor activity and selectivity of $RuPd_5/NH_2$-SiO_2 in the cleavage of CHPE (26% Conv. with 31% Sel.). Furthermore, DCHE cannot be converted on $RuPd_5/NH_2$-SiO_2 under current reaction conditions. This could exclude the reaction pathway via hydrogenolysis/hydrolysis of DCHE.[5c,11a] It can be concluded that the C-O bond of DPE is directly cleaved on $RuPd_5/NH_2$-SiO_2.

Table 1. The C-O bond cleavage of DPE over $RuPd_5/NH_2$-SiO_2 as a function of reaction time.[a]

T (min)	Product Sel. (%) [b]							Conv. (%)	Sel. (%) [c]
	CH	Bz	CHOH	CHO	PhOH	CHPE	DCHE		
3	4	40	29	20	7	~ 0	0	15	> 99
15	3	38	31	24	3	~1	0	71	99
30	14	20	49	15	0	1	0	89	99
45	24	4	69	2	0	1	0	97	99
60	29	0	71	0	0	1	0	99	99

[a]Reaction conditions: 110 °C, 0.22 mmol DPE, 0.022 mmol metals, 3 mL H_2O, 10 bar H_2. [b] CH (cyclohexane), Bz (benzene), CHOH (cyclohexanol), CHO (cyclohexanone), PhOH (phenol), DCHE (dicyclohexyl ether), CHPE ((cyclohexyloxy)benzene). [c]Monomers selectivity.

The hydrogenolysis of DPE is the main reaction pathway for $RuPd_5/NH_2$-SiO_2 and Ru/NH_2-SiO_2 at the initial time (88% vs. 68%, similar conversion of ~15%) (**Figure 3A-B**). With the

reaction time prolonging, the selectivity to hydrogenolysis products decreased accompanied with the selectivity to hydrolysis products increasing for the two catalysts. Finally, the products ratio of hydrogenolysis to hydrolysis on $RuPd_5/NH_2$-SiO_2 and Ru/NH_2-SiO_2 reached to 3:2 and 2.4:2, respectively. The higher hydrogenolysis ratio on $RuPd_5/NH_2$-SiO_2 may be related to its higher H_2 dissociation ability and lower aromatic ring hydrogenation ability (**Table S11**). No conversion was obtained on $RuPd_5/NH_2$-SiO_2 in the N_2 atmosphere, showing the important role of H_2 in the catalysis. Only hydrogenolysis (65%) and hydrogenation (35%) products was obtained on $RuPd_5/NH_2$-SiO_2 using isopropanol as solvent (**Table S6**). The hydrogenolysis selectivity in water and in isopropanol on $RuPd_5/NH_2$-SiO_2 was similar, indicating that the water does not involve in the hydorgenolysis reaction pathway.

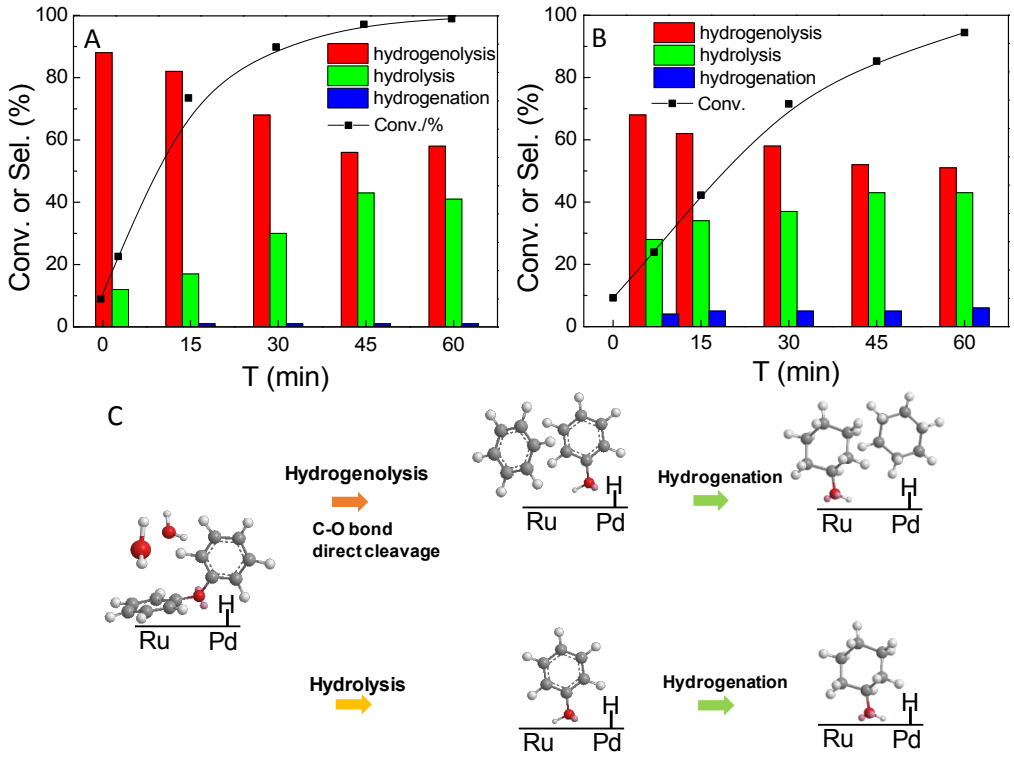

Figure 3. Reaction profiles of C-O bond cleavage of DPE with the reaction time catalyzed by (A) $RuPd_5/NH_2$-SiO_2 and (B) Ru/NH_2-SiO_2. Reaction conditions: 110 °C, 0.22 mmol DPE, 0.022 mmol metals, 3 mL H_2O, 10 bar H_2. Selctivity to hydrogenolysis = 2 × (CH + Bz), selectivity to

hydrolysis = (PhOH + CHO + CHOH) – (CH + Bz). Abbreviation see Table 1. (C) Proposed reaction pathways for the DPE cleavage over $RuPd_5/NH_2$-SiO_2 in water.

Combining the above results, the possible reaction pathway on $RuPd_5/NH_2$-SiO_2 can be proposed as follows (**Figure 3C**). Firstly, H_2 is activated on Pd sites to generate active H species. Meanwhile, DPE is chemisorbed on Ru active sites via strong π interactions between one aromatic ring and *d*-states of the metal (possibly the most stable adsorption mode).[15b,35] Subsequently, the active H species spilled over to Ru sites to attack C-O bond,[36] consequently resulting in the direct C-O bond scission. The produced monomers transferred to metal surface to be hydrogenated for the formation saturated cyclohexane and cyclohexanol.

The organosolv lignin extracted from beech sawdust was used to investigate the catalytic performance of RuPd alloy. The reaction was performed under H_2 atmosphere (30 bar) at 150 ^oC for 10 h. 2D ^{13}C-^1H heteronuclear single quantum correlation (HSQC) NMR experiments were conducted to monitor the cleavage of the characteristic interconnecting bonds within lignin (**Figure S13**). After reaction, the signals which can be ascribed to the phenylcoumaran structures B (B_α, B_β and B_γ) and the resinol structures C (C_α, C_β and C_γ) significantly reduced, showing $RuPd_5/NH_2$-SiO_2 could be able to degrade the lignin at mild conditions. However, most of the β-O-4 linkages A- and A'-signals still present, suggesting the β-O-4 bonds cannot be easily cleaved under this conditions.

The recycle stability of $RuPd_5/NH_2$-SiO_2 was tested in the cleavage of DPE (**Figure S14**). The result revealed that $RuPd_5/NH_2$-SiO_2 could be stably reusable for at least 5 times. After 5 cycles, $RuPd_5/NH_2$-SiO_2 could still afforded 94% conversion. TEM results shows that no aggregation of metal NPs could be observed. Furthermore, no traces of leached Ru or Pd species were detected in the reaction filtrate, demonstrating its good recyclability stability under current conditions.

3. CONCLUSION

In summary, the RuPd bimetallic NPs (2.1 nm) uniformly dispersed on amine-rich silica hollow nanospheres (NH_2-SiO_2) could efficiently catalyze the H_2 assisted C-O bond cleavage of diphenyl ether in H_2O even at temperature as low as 80 ^oC. The obvious volcano relationship between conversion and Ru content suggested the synergistic effect of Ru and Pd. The TOF of RuPd NPs increased remarkably as the Ru contents decreased, indicating that the isolated Ru sites were more active than Ru crystallites. The studies show that the unique catalytic performance of RuPd bimetallic NPs was strongly related with the optimized H_2 activation ability and the site isolation of Ru resulting from the alloying effect. The excellent catalytic performance and good recyclability make the $RuPd_5/SiO_2$-NH_2 catalyst attractive for both fundamental research and practical applications.

4. EXPERIMENT SECTION

Chemicals and agents. All materials were of analytical grade and used as received without any further purication. Diphenyl ether was purchased from J&K Chemicals. Phenol and decane were obtained from TCI Chemicals (Shanghai). Fluorocarbon surfactant (FC4) was bought from YickVic Chemicals (Hong Kong). Cyclohexyloxybenzene were purchered from Fluorochem (UK). Oxydicyclohexane were synthesized according to the previous method.[5c] (3-Amineпropyl)triethoxysilane (APTES), tetraethoxysilane (TEOS), cetyltrimethylammonium bromide (CTAB) and other reagents were purchased from Shanghai Chemical Reagent, Inc. of the Chinese Medicine Group.

Preparation of amine-rich mesoporous silica hollow nanospheres (NH_2-SiO_2). **Step1**. Tetraethoxysilane (TEOS) (0.25 mL) was added into 23 mL of aqueous solution containing 0.05 g of CTAB and 0.18 mL of NaOH solution (2.0 M) under slow stirring. Then, 0.2 mL of ethyl

acetate was successively added to the solution, and the synthetic medium was kept at 70 °C for 30 min without stirring. **Step 2**. 60 mL of aqueous solution (40 mL) with ethanol (20 mL), CTAB (0.15 g), and $NH_3 \cdot H_2O$ (0.5 mL, 25 wt%) was added to the above mixture. After cooling down to 38 °C, the reaction mixture was kept at this temperature with stirring for 30 min, then TEOS (0.25 mL) was added under stirring. The mixture was stirred for 1 h followed by the addition of 1.5 mL of aqueous solution with FC4 (0.02 g), CTAB (0.04 g), and $NH_3 \cdot H_2O$ (0.1 mL, 25 wt%). **Step 3**. Then, 1.33 mL of ethanol solution with APTES (0.33 mL) was added under vigorous stirring. After stirring for 1 h, the reaction mixture was stirred at 80 °C for 10 h with the stopper open to evaporate the solvent. The powder product was collected by filtration and dried at room temperature. To remove the surfactant, the as-synthesized materials (1 g) was dispersed in 120 mL of ethanol (95%) with ammonium nitrate (80 mg) and sirred at 60 °C for 20 min. This process was repeated for three times.

Preparation of $RuPd_x/NH_2$-SiO_2 via the impregnation method. Typically, 400 mg of NH_2-SiO_2 was dispersed in 2 mL of deionized water in a centrifuge tube under ultrasound. Then desired amount of Na_2PdCl_4 and $RuCl_3$ aqueous solution (0.01 g mL^{-1}) was added into the tube successively. After ultrasound treatment for 10 min, a freshly prepared $NaBH_4$ aqueous solution (7.5 mg mL^{-1}) was added dropwise. The brownish red colour transformed into dark gray. After ultrasound treatment for another 30 min, the mixture was filtered and the black powder product was washed with deionized water and EtOH for several times. After drying in an oven at 60 °C overnight, $RuPd_x/NH_2$-SiO_2 was obtained where x refers to molar ratio of Pd per Ru. $RuAu_x/NH_2$-SiO_2 bimetallic NPs were prepared in a similar method with $RuPd_5/NH_2$-SiO_2 except that $HAuCl_4$ was used.

The reaction of diphenyl ether. In a typical experiment, a desired amount of solid catalyst (0.022 mmol of metals) was added in an ampoule tube, followed by the addition of diphenyl ether (0.22 mmol) (S/C=10) and 3 mL of water. The ampoule tube was loaded into a stainless steel autoclave (300 mL) with a thermocouple probed detector. After purging with hydrogen for six times, the final pressure was adjusted to 10 bar and the reactor was heated to 110 ^{o}C with vigorous stirring. After reaction, the reactor was quenched to ambient temperature using cooling water, and the organic products were extracted using ethyl acetate (5 mL). The water phase and oil phase were respectively analyzed by an Agilent 7890B GC equipped with an Agilent J&W GC HP-INNOWax capillary column (30 m × 0.32 mm × 0.5 μm). Conversion and selectivity were determined using n-decane and EtOH as the internal standard respectively for oil and water phase and defined as **eqs 1-5**. The monomers refer to benzene, cyclohexane, phenol, cyclohexanone and cyclohexanol. The dimers refer to (cyclohexyloxy)benzene and dicyclohexyl ether. The carbon balance for all the reactions was > 90%.

$$\text{Conversion (\%)} = \frac{6 * (\text{The amount of monomers/mmol}) + 12 * (\text{The amount of dimers/mmol})}{12 * (\text{The initial amount of diphenyl ether/mmol})} * 100 \quad (1)$$

$$\text{Selectivity to hydrogenolysis (\%)} = 2 * \frac{6 * (\text{The amount of benzene and cyclohexane/mmol})}{6 * (\text{The amount of monomers/mmol}) + 12 * (\text{The amount of dimers/mmol})} * 100 \quad (2)$$

$$\text{Selectivity to hydrogenation (\%)} = \frac{12 * (\text{The amount of dimers/mmol})}{6 * (\text{The amount of monomers/mmol}) + 12 * (\text{The amount of dimers/mmol})} * 100 \quad (3)$$

$$\text{Selectivity to hydrolysis (\%)} = \frac{6 * (\text{The amount of phenol, cyclohexanone and cyclohexol/mmol}) - 6 * (\text{The amount of benzene and cyclohexane/mmol})}{6 * (\text{The amount of monomers/mmol}) + 12 * (\text{The amount of dimers/mmol})} * 100 \quad (4)$$

$$\text{Selectivity to the C - O bond (\%)} = (\text{Selectivity to hydrogenolysis/\%}) + (\text{Selectivity to hydrolysis/\%}) \quad (5)$$

Characterization

Transmission electron microscopy (TEM) was performed on a HITACHI 7700 at an acceleration voltage of 100 kV. Scanning transmission electron microscopy (STEM) was undertaken on a HITACHI S-5500 scanning electron microscope operating at an acceleration

voltage of 1-20 kV. The EDS mapping were obtained using a JEOL F200. 2D ^{13}C-^{1}H heteronuclear single quantum correlation (HSQC) NMR spectra were recorded at 25 ^{o}C using a Bruker Avance III HD 700 MHz spectrometer. 60 mg sample was dispersed in 0.5 mL of DMSO-d_6. The central DMSO solvent peak was used as an internal chemical shift reference point (δ_C/δ_H 39.52/2.49).[37] The N_2 adsorption-desorption experiments were performed at 77 K using a Micromeritrics ASAP 2020. Samples were degassed at 120 ^{o}C for 6 hours prior to the measurements. FT-IR spectra were collected with a Nicolet Nexus 470 IR spectrometer (KBr pellets were prepared) in the range of 400-4000 cm^{-1}. The thermogravimetric analysis (TGA) was performed using a NETZSCH STA 449F3 analyzer from 30 ^{o}C to 900 ^{o}C at a heating rate of 10 $^{o}C \cdot min^{-1}$ under air atmosphere. The metal content was determined by PLASAMSPEC-II inductively coupled plasma atomic emission spectrometry (ICP-AES). X-ray photoelectron spectroscopy (XPS) was recorded on VG ESCALAB MK_2 apparatus using Al K_α (h_λ = 1486.6 eV) as the excitation light source. The peaks in the spectra were fitted by using the shareware program XPS-PEAK with Gaussian-Lorentzian peak shapes and a Shirley background. The binding energies are corrected with reference to the C 1s line at 284.6 eV.

In situ FT-IR of CO adsorption were collected on a Bruker EQUINOX 55 infrared spectrometer with a DTGS detector. Prior to CO chemisorption, as-prepared samples were pretreated at 200 ^{o}C under flowing H_2 atmosphere (20 mL min^{-1}) for 1 h, followed by evacuation at room temperature for 1 h, then cooled down to room temperature. After pretreatment, a background spectrum was collected from samples and subtracted automatically from subsequent spectra. CO adsorption experiments were carried out sequentially on a single sample. Gas-phase CO spectra were collected at the same pressure and subtracted from the corresponding sample spectra.[15d]

H_2-D_2 exchange reactions were carried out in a flow quartz reactor at 22 °C.[38] The formation rate of HD was measured by mass signal intensity (ion current). Before the test, the catalysts were heated in H_2 (10 mL min^{-1}) at 200 °C for 20 min. After the sample was cooled at room temperature, D_2 (10 mL min^{-1}) mixed with H_2 was passed through the sample. The gas hourly space velocity (GHSV) is 1.16×10^8 $mL \cdot h^{-1} \cdot g_{metal}^{-1}$. Under these conditions, the H_2-D_2 exchange conversions were always kept below 15% for calculation of turnover frequency (TOF).[38b] Products (HD, H_2, and D_2) were analyzed with an online mass spectrometer (GAM200, InProcess Instruments). The mass/charge ratio (m/z) values used are 2 for H_2, 4 for D_2, and 3 for HD. The background HD exchanges from the corresponding support were deducted from the results.

Characterization of NH_2-SiO_2.

The results of TEM and HRSEM characterizations show that NH_2-SiO_2 is composed of mono-dispersed nanospheres with particle size in the range of 100~200 nm and has a rough surface formed with connected nanoparticles with size of 10-25 nm (**Figure S1**). A broken nanosphere chosen intentionally clearly confirmed the hollow nanostructures (**Figure S1B**). NH_2-SiO_2 has the BET surface area of 156 m^2 g^{-1} with pore size distribution centered at 15 nm derived mainly from inter void space of the connected nanoparticles (**Table S1**). The solid-state ^{13}C CP/MAS NMR spectrum displays the chemical shifts at 8.8 ppm, 20.8 ppm and 40.9 ppm, which could be assigned to C_1, C_2 and C_3 of $-C^1H_2C^2H_2C^3H_2NH_2$, suggesting the successful incorporation of amine groups (**Figure S2A**). The solid-state ^{29}Si NMR spectrum exhibits both T sites (-69.9 ppm for T_3) and Q sites (-101.7 ppm for Q_3 and -113.8 ppm for Q_4) with T/(Q+T) ratio of about 22.4 %, showing the integration of APTES in NH_2-SiO_2 hollow nanospheres (**Figure S2B**). FT-IR spectrum of NH_2-SiO_2 clearly show the vibration peaks assigned to propyl groups at 2937 cm^{-1}

(υ_{C-H}) and 1385 cm^{-1} (δ_{C-H}) and amine group at 3441 cm^{-1} (υ_{N-H}) and 1558 cm^{-1} (δ_{N-H}) (**Figure S3A**). On the basis of the TG analysis (**Figure S3B**), the weight loss of 22.9 wt% in the range of 250 to 750 ^{o}C could be assigned to the content of amine groups, which corresponds to amine amount of 3.95 mmol g^{-1}. The C, H, N elemental analysis affords N content of 5.4 wt%. The calculated amine amount is 3.85 mmol g^{-1}, which is consistent with the TG analysis result. The above results confirm the formation of porous silica hollow nanospheres rich in amine group via one-pot synthesis method.

ASSOCIATED CONTENT

Supporting Information

The Supporting Information is available free of charge on the xxx.

TEM and STEM images, ^{13}C CP/MAS NMR spectrum, ^{29}Si MAS NMR spectrum, FT-IR spectrum, TG analysis results and physical parameters of NH_2-SiO_2, TEM images of $RuPd_{0.33}/NH_2$-SiO_2, $RuPd_1/NH_2$-SiO_2, (C) $RuPd_9/NH_2$-SiO_2 and (D) $RuPd_{20}/NH_2$-SiO_2, EDS results of $RuAu_5/NH_2$-SiO_2, arrhenius plots of Ru/NH_2-SiO_2 and $RuPd_5/NH_2$-SiO_2, XPS results of $RuPd_x/NH_2$-SiO_2 and $RuAu_x/NH_2$-SiO_2, in situ FT-IR spectra of CO adsorption results on $RuAu_x/NH_2$-SiO_2, $RuPd_9/NH_2$-SiO_2 and $RuPd_{20}/NH_2$-SiO_2, the results of H_2-D_2 exchange reactions and the reusability results.

AUTHOR INFORMATION

Corresponding Author

yangqh@dicp.ac.cn;

canli@dicp.ac.cn;

Author Contributions

M. G. did all the experiment and wrote the manuscript, J. P. designed and synthesized the material, and Q. Y. and C. L. made the research plan, supervised the research, and organized the paper.

Notes

The authors declare no competing financial interest.

ACKNOWLEDGMENT

This work was financially supported by the National Key R&D Program of China, 2017YFB0702800, the Natural Science Foundation of China (No. 21733009, 21232008, 21621063) and the Strategic Priority Research Program of the Chinese Academy of Sciences Grant No. XDB17020200.

REFERENCES

1. (a) Boerjan, W.; Ralph, J.; Baucher, M. Lignin Biosynthesis. *Annu. Rev. Plant Biol.* **2003**, *54*, 519-546. (b) Zakzeski, J.; Bruijnincx, P. C. A.; Jongerius, A. L.; Weckhuysen, B. M. The Catalytic Valorization of Lignin for the Production of Renewable Chemicals. *Chem. Rev.* **2010**, *110*, 3552-3599.
2. (a) Li, C.; Zhao, X.; Wang, A.; Huber, G. W.; Zhang, T. Catalytic Transformation of Lignin for the Production of Chemicals and Fuels. *Chem. Rev.* **2015**, *115*, 11559-11624. (b) Meng, Q.; Hou, M.; Liu, H.; Song, J.; Han, B. Synthesis of Ketones from Biomass-Derived Feedstock. *Nat. Commun.* **2017**, *8*, 14190. (c) Shuai, L.; Amiri, M. T.; Questell-Santiago, Y. M.; Heroguel, F.; Li, Y.; Kim, H.; Meilan, R.; Chapple, C.; Ralph, J.; Luterbacher, J. S. Formaldehyde Stabilization Facilitates Lignin Monomer Production during Biomass Depolymerization. *Science* **2016**, *354*, 329-333. (d) Parsell, T.; Yohe, S.; Degenstein, J.;

Jarrell, T.; Klein, L.; Gencer, E.; Hewetson, B.; Hurt, M.; Kim, J.; Choudhari, H.; Saha, B.; Meilan, R.; Mosier, N.; Ribeiro, F.; Delgass, W.; Chapple, C.; Kenttämaa, H.; Agrawal, R.; Abu-Omar, M. A Synergistic Biorefinery Based on Catalytic Conversion of Lignin Prior to Cellulose Starting from Lignocellulosic Biomass. *Green Chem.* **2015**, *17*, 1492-1499. (e) Upton, B. M.; Kasko, A. M. Strategies for the Conversion of Lignin to High-Value Polymeric Materials: Review and Perspective. *Chem. Rev.* **2015**, *116*, 2275-2306. (f) Deng, W.; Zhang, H.; Xue, L.; Zhang, Q.; Wang, Y. Selective Activation of the C-O Bonds in Lignocellulosic Biomass for the Efficient Production of Chemicals. *Chin. J. Catal.* **2015**, *36*, 1440-1460.

3. (a) Alonso, D. M.; Wettstein, S. G.; Dumesic, J. A. Bimetallic Catalysts for Upgrading of Biomass to Fuels and Chemicals. *Chem. Soc. Rev.* **2012**, *41*, 8075-8098. (b) Van den Bosch, S.; Schutyser, W.; Vanholme, R.; Driessen, T.; Koelewijn, S. F.; Renders, T.; De Meester, B.; Huijgen, W. J. J.; Dehaen, W.; Courtin, C. M.; Lagrain, B.; Boerjan, W.; Sels. B. F. Reductive Lignocellulose Fractionation into Soluble Lignin-Derived Phenolic Monomers and Dimers and Processable Carbohydrate Pulps. *Energy Environ. Sci.* **2015**, *8*, 1748-1763. (c) Yan, N.; Zhao, C.; Dyson, P. J.; Wang, C.; Liu, L.; Kou, Y. Selective Degradation of Wood Lignin over Noble-Metal Catalysts in a Two-Step Process. *ChemSusChem* **2008**, *1*, 626-629. (d) Corma, A.; Iborra, S.; Velty, A. Chemical Routes for the Transformation of Biomass into Chemicals. *Chem. Rev.* **2007**, *107*, 2411-2502. (e) Wang, M.; Zhang, X.; Li, H.; Lu, J.; Liu, M.; Wang, F. Carbon Modification of Nickel Catalyst for Depolymerization of Oxidized Lignin to Aromatics. *ACS Catal.* **2018**, *8*, 1614-1620. (f) Song, Q.; Wang, F.; Xu, J. Hydrogenolysis of Lignosulfonate into Phenols over Heterogeneous Nickel Catalysts. *Chem. Commun.* **2012**, *48*, 7019-7021. (g) Zaheer, M.; Kempe, R. Catalytic Hydrogenolysis of Aryl

Ethers: A Key Step in Lignin Valorization to Valuable Chemicals. *ACS Catal.* **2015**, *5*, 1675-1684.

4. Luo, Y. R. Comprehensive Handbook of Chemical Bond Energies, CRC Press, 1 Edition, Boca Raton, FL, **2007**, pp. 331.
5. (a) Saper, N. I.; Hartwig, J. F. Mechanistic Investigations of the Hydrogenolysis of Diaryl Ethers Catalyzed by Nickel Complexes of N-Heterocyclic Carbene Ligands. *J. Am. Chem. Soc.* **2017**, *139*, 17667-17676. (b) Wang, M.; Shi, H.; Camaioni, D. M.; Camaioni, D. M.; Lercher, J. A. Palladium-Catalyzed Hydrolytic Cleavage of Aromatic C-O Bonds. *Angew. Chem. Int. Ed.* **2017**, *56*, 2110-2114. (c) He, J.; Zhao, C.; Mei, D.; Lercher, J. A. Mechanisms of Selective Cleavage of C-O bonds in Di-aryl Ethers in Aqueous Phase. *J. Catal.* **2014**, *309*, 280-290.
6. Sergeev, A. G.; Hartwig, J. F. Selective, Nickel-Catalyzed Hydrogenolysis of Aryl Ethers. *Science* **2011**, *332*, 439-443.
7. (a) Wang, M.; Guti é rrez, O. Y.; Camaioni, D. M.; Lercher, J. A. Palladium-Catalyzed Reductive Insertion of Alcohols into Aryl Ether Bonds. *Angew. Chem. Int. Ed.* **2018**, *57*, 3747-3751. (b) Chen, L.; Xin, J.; Ni, L.; Dong, H.; Yan, D.; Lu, X.; Zhang, S. Conversion of Lignin Model Compounds under Mild Conditions in Pseudo-Homogeneous Systems. *Green Chem.* **2016**, *18*, 2341-2352. (c) Shao, Y.; Xia, Q.; Liu, X.; Lu, G.; Wang, Y. Pd/Nb_2O_5/SiO_2 Catalyst for the Direct Hydrodeoxygenation of Biomass-Related Compounds to Liquid Alkanes under Mild Conditions. *ChemSusChem* **2015**, *8*, 1761-1767.
8. (a) Guan, W.; Chen, X.; Jin, S.; Li, C.; Tsang, C.; Liang, C. Highly Stable Nb_2O_5-Al_2O_3 Composites Supported Pt Catalysts for Hydrodeoxygenation of Diphenyl Ether. *Ind. Eng. Chem. Res.* **2017**, *56*, 14034-14042. (b) Chen, L.; Fink, C.; Fei, Z.; Dyson, P. J.; Laurenczy,

G. An Efficient Pt Nanoparticle-Ionic Liquid System for the Hydrodeoxygenation of Bio-Derived Phenols under Mild Conditions. *Green Chem.* **2017**, *19*, 5435-5441.

9. (a) Chatterjee, M.; Ishizaka, T.; Suzuki, A.; Kawanami, H. An Efficient Cleavage of the Aryl Ether C-O Bond in Supercritical Carbon Dioxide-Water. *Chem. Commun.* **2013**, *49*, 4567-4569. (b) Chatterjee, M.; Chatterjee, A.; Ishizaka, T.; Kawanami, H. Rhodium-Mediated Hydrogenolysis/Hydrolysis of the Aryl Ether Bond in Supercritical Carbon Dioxide/Water: An Experimental and Theoretical Approach. *Catal. Sci. Technol.* **2015**, *5*, 1532-1539. (c) Chatterjee, M.; Ishizaka, T.; Kawanami, H. Hydrogenolysis/Hydrogenation of Diphenyl Ether as a Model Decomposition Reaction of Lignin from Biomass in Pressurized CO_2/Water Condition. *Catal. Today* **2017**, *281*, 402-409. (d) Song, Y.; Chia, S. H.; Sanyal, U.; Gutierreza, O.; Lercher, J. A. Integrated Catalytic and Electrocatalytic Conversion of Substituted Phenols and Diaryl Ethers. *J. Catal.* **2016**, *344*, 263-272.
10. (a) Yao, G.; Wu, G.; Dai, W.; Guan, N.; Li, L. Hydrodeoxygenation of Lignin-Derived Phenolic Compounds over Bi-Functional Ru/H-Beta under Mild Conditions. *Fuel* **2015**, *150*, 175-183. (b) Long, J.; Xu, Y.; Wang, T.; Yuan, Z.; Shu, R.; Zhang, Q.; Ma, L. Efficient Base-Catalyzed Decomposition and in Situ Hydrogenolysis Process for Lignin Depolymerization and Char Elimination. *Appl. Energ.* **2015**, *141*, 70-79. (c) Wu, H.; Song, J.; Xie, C.; Wu, C.; Chen, C.; Han, B. Efficient and Mild Transfer Hydrogenolytic Cleavage of Aromatic Ether Bonds in Lignin-Derived Compounds over Ru/C. *ACS Sustainable Chem. Eng.* **2018**, *6*, 2872-2877. (d) Konnerth, H.; Zhang, J.; Ma, D.; Pretchtl, M, Yan, N. Base Promoted Hydrogenolysis of Lignin Model Compounds and Organosolv Lignin over Metal Catalysts in Water. *Chem. Eng. Sci.* **2015**, *123*, 155-163. (e) Gómez-Monedero, B.; Ruiz, M. P.; Bimbela, F.; Faria, J. Selective Hydrogenolysis of α-O-4, β-O-4, 4-O-5 C-O Bonds of

Lignin-Model Compounds and Lignin-Containing Stillage Derived from Cellulosic Bioethanol Processing. *Appl. Catal. A-Gen.* **2017**, *541*, 60-76.

11. (a) He, J.; Zhao, C.; Lercher, J. A. Ni-Catalyzed Cleavage of Aryl Ethers in the Aqueous Phase. *J. Am. Chem. Soc.* **2012**, *134*, 20768-20775. (b) Stavila, V.; Parthasarathi, R.; Davis, R. W.; Gabaly, F. E.; Sale, K. L.; Simmons, B. A.; Singh, S.; Allendorf, M. D. MOF-Based Catalysts for Selective Hydrogenolysis of Carbon-Oxygen Ether Bonds. *ACS Catal.* **2015**, *6*, 55-59. (c) Zaheer, M.; Hermannsdörfer, J.; Kretschmer, W. P.; Motz, G.; Kempe, R. Robust Heterogeneous Nickel Catalysts with Tailored Porosity for the Selective Hydrogenolysis of Aryl Ethers. *ChemCatChem* **2014**, *6*, 91-95. (d) Molinari, V.; Giordano, C.; Antonietti, M.; Esposito, D. Titanium Nitride-Nickel Nanocomposite as Heterogeneous Catalyst for the Hydrogenolysis of Aryl Ethers. *J. Am. Chem. Soc.* **2014**, *136*, 1758-1761. (e) Wang, X.; Rinaldi, R. Solvent Effects on the Hydrogenolysis of Diphenyl Ether with Raney Nickel and Their Implications for the Conversion of Lignin. *ChemSusChem* **2012**, *5*, 1455-1466.
12. (a) Mauriello, F.; Paone, E.; Pietropaolo, R.; Balu, A. M.; Luque, R. Catalytic Transfer Hydrogenolysis of Lignin Derived Aromatic Ethers Promoted by Bimetallic Pd/Ni Systems. *ACS Sustainable Chem. Eng.* **2018**, *6*, 9269-9276. (b) Zhang, J.; Teo, J.; Chen, X.; Asakusa, H.; Takana, T.; Teramura, K.; Yan, N. A Series of NiM (M= Ru, Rh, and Pd) Bimetallic Catalysts for Effective Lignin Hydrogenolysis in Water. *ACS Catal.* **2014**, *4*, 1574-1583. (c) Pichaikaran S, Pandurangan A. Rh/Ni Wet-Impregnated Ia3d Mesostructured Aluminosilicate and r-GO Catalysts for Hydrodeoxygenation of Phenoxybenzene. *New J. Chem.* **2017**, *41*, 7893-7907. (d) Bulut, S.; Siankevich, S.; van Muyden, A. P.; Alexander, D. T. L.; Savoglidis, G.; Zhang, J.; Hatzimanikatis, V.; Yan, N.; Dyson, P. J. Efficient Cleavage

of Aryl Ether C-O linkages by Rh-Ni and Ru-Ni Nanoscale Catalysts Operating in Water *Chem. Sci.* **2018**, *9*, 5530-5535.

13. (a) Kobayashi, H.; Kusada, K.; Kitagawa, H. Creation of Novel Solid-Solution Alloy Nanoparticles on the Basis of Density-of-States Engineering by Interelement Fusion. *Acc. Chem. Res.* **2015**, *48*, 1551-1559. (b) Gao F, Goodman, D. W. P. Pd-Au Bimetallic Catalysts: Understanding Alloy Effects from Planar Models and (Supported) Nanoparticles. *Chem. Soc. Rev.* **2012**, *41*, 8009-8020.
14. (a) Zafeiratos, S.; Piccinin, S.; Teschner, D. Alloys in Catalysis: Phase Separation and Surface Segregation Phenomena in Response to the Reactive Environment. *Catal. Sci. Technol.* **2012**, *2*, 1787-1801. (b) Ponec, V. Alloy Catalysts: the Concepts. *Appl. Catal. A-Gen.* **2001**, *222*, 31-45. (c) Liu, J. Q.; Wang, A. Q.; Chi, Y. S.; Lin, H. P.; Mou, C. Y. Synergistic Effect in an Au-Ag Alloy Nanocatalyst: CO Oxidation. *J. Phys. Chem. B* **2005**, *109*, 40-43.
15. (a) Shao, Y.; Xia, Q.; Dong, L.; Liu, X.; Han, X.; Parker, S. F.; Cheng, Y.; Daemen, L. L.; Ramirez-Cuesta, A. J.; Yang, S.; Wang, Y. Selective Production of Arenes via Direct Lignin Upgrading over a Niobium-Based Catalyst. *Nat. Commun.* **2017**, *8*, 16104. (b) Nelson, R. C.; Baek, B.; Ruiz, P.; Goundie, B.; Brooks, A.; Wheeler, M. C.; Frederick, B. G.; Grabow, L. C.; Rachel Narehood Austin, R. N. Experimental and Theoretical Insights into the Hydrogen-Efficient Direct Hydrodeoxygenation Mechanism of Phenol over Ru/TiO_2. *ACS Catal.* **2015**, *5*, 6509-6523. (c) Adams, B. D.; Chen, A. The Role of Palladium in a Hydrogen Economy. *Mater. Today* **2011**, *14*, 282-289; (d) Guo, M.; Li, H.; Ren, Y.; Ren, X.; Yang, Q.; Li, C. Improving Catalytic Hydrogenation Performance of Pd Nanoparticles by Electronic Modulation Using Phosphine Ligands. *ACS Catal.* **2018**, *8*, 6476-6485.

16. (a) Guo, M.; Li, C.; Yang, Q. Accelerated Catalytic Activity of Pd NPs Supported on Amine-Rich Silica Hollow Nanospheres for Quinoline Hydrogenation. *Catal. Sci. Technol.* **2017**, *7*, 2221-2227. (b) Lan, G.; Zhang, X.; Zhang, X.; Li, M.; Li, Y.; Yang, Q. Yolk-Shell Nanospheres with Soluble Amino-Polystyrene as a Reservoir for Pd NPs. *RSC Adv.* **2015**, *5*, 35730-35736.

17. (a) Zheng, N,; Liu, P. Amine Facilitates the Synthesis of Silica-Supported Ultrasmall Bimetallic Nanoparticles. *Sci. China Mater.* **2018**, *61*, 1129-1131. (b) Wang, A.; Liu, Q.; Griffin, S.; Nicholls, A.; Regalbuto, J. R. *Science* **2017**, *358*, 1427-1430.

18. (a) Tripathi, S. N.; Bharadwaj, S. R.; Dharwadkar, S. R. T. The Pd-Ru System (Palladium-Ruthenium). *J. Phase equilib.* **1993**, *14*, 638-642. (b) Wu, D.; Zheng, Z.; Gao, S.; Cao, M.; Cao, R. Mixed-Phase PdRu Bimetallic Structures with High Activity and Stability for Formic Acid Electrooxidation. *Phys. Chem. Chem. Phys.* **2012**, *14*, 8051-8057. (c) Wu, Y.; Li, Y. *Sci. China Mater.* **2015**, 58, 3-4.

19. (a) Strasser, P.; Koh, S.; Anniyev, T.; Greeley, J.; More, K.; Yu, C.; Liu, Z.; Kaya, S.; Nordlund, D.; Ogasawara, H.; Toney, M.F.; Nilsson, A. Lattice-Strain Control of the Activity in Dealloyed Core-Shell Fuel Cell Catalysts. *Nat. Chem.* **2010**, *2*, 454-460. (b) Kitchin, J. R.; Nørskov, J. K.; Barteau, M. A.; Chen, J. G. Role of Strain and Ligand Effects in the Modification of the Electronic and Chemical Properties of Bimetallic Surfaces. *Phys. Rev. Lett.* **2004**, *93*, 156801.

20. (a) Kusada, K.; Kobayashi, H.; Ikeda, R.; Kubota, Y.; Takata, M.; Toh, S.; Yamamoto, T.; Matsumura, S.; Sumi, N.; Sato, K.; Nagaoka, K.; Kitagawa, H. Solid Solution Alloy Nanoparticles of Immiscible Pd and Ru Elements Neighboring on Rh: Changeover of the Thermodynamic Behavior for Hydrogen Storage and Enhanced CO-Oxidizing Ability. *J. Am.*

Chem. Soc. **2014**, *136*, 1864-1871. (b) Tang, M.; Mao, S.; Li, M.; Wei, Z.; Xu, F.; Li, H.; Wang, Y. RuPd Alloy Nanoparticles Supported on N-doped Carbon as an Efficient and Stable Catalyst for Benzoic Acid Hydrogenation. *ACS Catal.* **2015**, *5*, 3100-3107.

21. (a) Wu, D.; Kusada, K.; Kitagawa, H. Recent Progress in the Structure Control of Pd-Ru Bimetallic Nanomaterials. *Sci. Technol. Adv. Mat.* **2016**, *17*, 583-596. (b) Wu, D.; Cao, M.; Shen, M.; Cao, R. Sub-5 nm Pd-Ru Nanoparticle Alloys as Efficient Catalysts for Formic Acid Electrooxidation. *ChemCatChem* **2014**, *6*, 1731-1736.
22. Gao, F.; Wang, Y.; Goodman, D. W. CO Oxidation over AuPd (100) from Ultrahigh Vacuum to Near-Atmospheric Pressures: the Critical Role of Contiguous Pd Atoms. *J. Am. Chem. Soc.* **2009**, *131*, 5734-5735.
23. (a) Chin, S. Y.; Williams, C. T.; Amiridis, M. D. FTIR Studies of CO Adsorption on Al_2O_3- and SiO_2-Supported Ru Catalysts. *J. Phys. Chem. B* **2006**, *110*, 871-882. (b) Hadjiivanov, K.; Lavalley, J. C.; Lamotte, J.;Mauge, F.; Saint-Just, J.; Che, M. FTIR Study of CO Interaction with Ru/TiO_2 Catalysts. *J. Catal.* **1998**, *176*, 415-425.
24. (a) Nikolla, E.; Schwank, J.; Linic, S. Measuring and Relating the Electronic Structures of Nonmodel Supported Catalytic Materials to Their Performance. *J. Am. Chem. Soc.* **2009**, *131*, 2747-2754. (b) Ruban, A.; Hammer, B.; Stoltze, P.; Skriver, H. L.; Norskov, J. K. Surface Electronic Structure and Reactivity of Transition and Noble Metals. *J. Mol. Catal. A-Chem.* **1997**, *115*, 421-429.
25. (a) Stamenkovic, V. R.; Mun, B. S.; Arenz, M.; Mayrhofer, K. J. J.; Lucas, C. A.; Wang, G.; Ross, P. N.; Markovic, N. M. Trends in Electrocatalysis on Extended and Nanoscale Pt-Bimetallic Alloy Surfaces. *Nat. Mater.* **2007**, *6*, 241-247. (b) Li, X.; Wang, X.; Liu, M.; Liu,

H.; Chen, Q.; Yin, Y.; Jin, M. Construction of Pd-M (M = Ni, Ag, Cu) Alloy Surfaces for Catalytic Applications. *Nano Res.* **2018**, *11*, 780-790.

26. (a) Mao, J.; Chen, W.; Sun, W.; Chen, Z.; Pei, J.; He, D.; Lv, C.; Wang, D.; Li, Y. Rational Control of the Selectivity of a Ruthenium Catalyst for Hydrogenation of 4-Nitrostyrene by Strain Regulation. *Angew Chem. Int. Ed.* **2017**, *129*, 12133-12137. (b) Feng, Q.; Zhao, S.; Wang, Y.; Dong, J.; Chen, W.; He, D.; Wang, D.; Yang, J.; Zhu, Y.; Zhu, H.; Gu, L.; Li, Z.; Liu, Y.; Yu, R.; Li, J.; Li, Y. Isolated Single-Atom Pd Sites in Intermetallic Nanostructures: High Catalytic Selectivity for Semihydrogenation of Alkynes. *J. Am. Chem. Soc.* **2017**, *139*, 7294-7301.
27. (a) Galvagno, S., Schwank, J.; Parravano, G.; Grabassi, F.; Marzi, A.; Tauszik, G. R. Bimetallic Ru-Au Catalysts: Effect of the Support. *J. Catal.* **1981**, *69*, 283-291. (b) Okamoto, H.; Massalski, T. B. The Au-Ru (Gold-Ruthenium) System. *Bulletin of Alloy Phase Diagrams* **1984**, *5*, 388-390.
28. Calzada, L. A.; Collins, S. E.; Han, C. W.; Ortalan, V.; Zanella, R. Synergetic Effect of Bimetallic Au-Ru/TiO_2 Catalysts for Complete Oxidation of Methanol. *Appl. Catal. B-Environ.* **2017**, *207*, 79-92.
29. (a) Pfnür, H.; Menzel, D.; Hoffmann, F. M.; Ortega, A.; Bradshaw, A. M. High Resolution Vibrational Spectroscopy of CO on Ru (001): The Importance of Lateral Interactions. *Surf. Sci.* **1980**, *93*, 431-452. (b) Persson, B. N. J.; Hoffmann, F. M.; Ryberg, R. Influence of Exciton Motion on the Shape of Optical Absorption Lines: Applications to Vibrations at Surfaces. *Phys. Rev. B* **1986**, *34*, 2266. (c) Hoffmann, F. M.; Persson, B. N. J. Vibrational Dephasing of Terminally Bonded CO on Ru (001). *Phys. Rev. B* **1986**, *34*, 4354.

30. (a) Shastri, A. G.; Schwank, J. Metal Dispersion of Bimetallic Catalysts via Stepwise Chemisorption and Surface Titration: I. Ru-Au/SiO_2. *J. Catal.* **1985**, *95*, 271-283. (b) Maris, E. P.; Ketchie, W. C.; Murayama, M.; Davis, R. J. Glycerol Hydrogenolysis on Carbon-Supported PtRu and AuRu Bimetallic Catalysts. *J. Catal.* **2007**, *251*, 281-294. (c) Prati, L.; Porta, F.; Wang, D.; Villa, A. Ru Modified Au Catalysts for the Selective Oxidation of Aliphatic Alcohols. *Catal. Sci. Technol.* **2011**, *1*, 1624-1629.

31. (a) Kyriakou, G.; Boucher, M. B.; Jewell, A. D.; Lewis, E. A.; Lawton, T. J.; Baber, A. E.; Tierney, H. L.; Flytzani-Stephanopoulos, M.; Sykes, E. C. H. Isolated Metal Atom Geometries as a Strategy for Selective Heterogeneous Hydrogenations. *Science* **2012**, *335*, 1209-1212. (b) Teschner1, D.; Borsodi1, J.; Wootsch, A.; Révay, Z.; Hävecker, M.; Knop-Gericke1, A.; Jackson, S. D.; Schlögl, R. The Roles of Subsurface Carbon and Hydrogen in Palladium-Catalyzed Alkyne Hydrogenation. *Science* **2008**, *320*, 86-89.

32. (a) Greeley, J.; Mavrikakis, M. Surface and Subsurface Hydrogen: Adsorption Properties on Transition Metals and Near-Surface Alloys. *J. Phys. Chem. B* **2005**, *109*, 3460-3471. (b) Greeley, J.; Mavrikakis, M. Alloy Catalysts Designed from First Principles. *Nat. Mater.* **2004**, *3*, 810-815.

33. Fujitani, T.; Nakamura, I.; Akita, T.; Okumura, M.; Haruta, M. Hydrogen Dissociation by Gold Clusters. *Angew. Chem. Int. Ed.* **2009**, *48*, 9515-9518.

34. (a) Ge, J.; He, D.; Chen, W.; Ju, H.; Zhang, H.; Chao, T.; Wang, X.; You, R.; Lin, Y.; Wang, Y.; Zhu, J.; Li, H.; Xiao, B.; Huang, W.; Wu, Y.; Hong, X.; Li, Y. Atomically Dispersed Ru on Ultrathin Pd Nanoribbons. *J. Am. Chem. Soc.* **2016**, *138*, 13850-13853. (b) Amon, B.; Redlingshöfer, H.; Klemm, E.; Dieterich, E.; Emig, G. Kinetic Investigations of the

Deactivation by Coking of a Noble Metal Catalyst in the Catalytic Hydrogenation of Nitrobenzene Using a Catalytic Wall Reactor *Chem. Eng. Process* **1999**, *38*, 395-404.

35. Hensley, A. J. R.; Wang, Y.; McEwen, J. Adsorption of Phenol on Fe (110) and Pd (111) from First Principles. *Sur. Sci.* **2014**, *630*, 244-253.
36. (a) Christmann, K. Hydrogen Transfer on Metal Surfaces. *Hydrogen-Transfer Reactions*. **2006**, 751-786. (b) Marcinkowski, M. D.; Jewell, A. D.; Stamatakis, M.; Boucher, M. B.; Lewis, E. A.; Murphy, C. J.; Kyriakou, G.; Sykes, E. C. H. Controlling a spillover pathway with the molecular cork effect. *Nat. Mater.* **2013**, *12*, 523-528.
37. (a) Si, X.; Lu, F.; Chen, J.; Lu, R.; Huang, Q.; Jiang, H.; Taarning, E.; Xu, J. A Strategy for Generating High-Quality Cellulose and Lignin Simultaneously from Woody Biomass. *Green Chem.* **2017**, *19*, 4849-4857. (b) Luo, H.; Wang, L.; Li, G.; Shang, S.; Lv, Y.; Niu, J.; Gao, S. Nitrogen-Doped Carbon Modified Cobalt Nanoparticles Catalyzed Oxidative Cleavage of Lignin β-O-4 Model Compounds under Mild Conditions. *ACS Sustainable Chem. Eng.* **2018**. DOI: 10.1021/acssuschemeng.8b02802.
38. (a) Wang, J.; Li, G.; Li, Z.; Tang, C.; Feng, Z.; An, H.; Liu, H.; Liu, T. Li, C. A Highly Selective and Stable ZnO-ZrO_2 Solid Solution Catalyst for CO_2 Hydrogenation to Methanol. *Sci. Adv.* **2017**, *3*, e1701290. (b) Bai, L.; Wang, X.; Chen, Q.; Ye, Y.; Zheng, H.; Guo, J.; Yin, Y.; Gao, C. Explaining the Size Dependence in Platinum-Nanoparticle-Catalyzed Hydrogenation Reactions. *Angew. Chem. Int. Ed.* **2016**, *55*, 15656-15661.

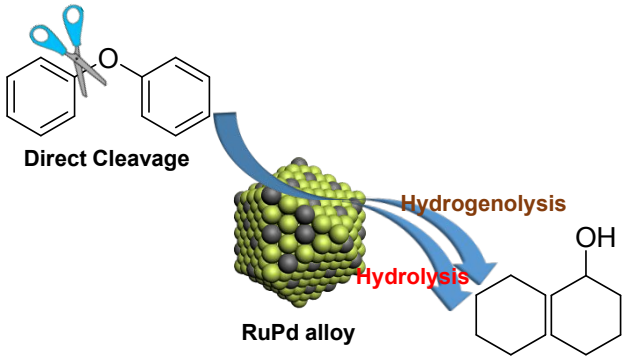
O
Direct Cleavage
Hydrogenolysis
OH
Hydrolysis
RuPd alloy